Inorganic Chemistry

pubs.acs.org/IC

Article

Insights on the Structure in Solution of Paramagnetic Ln^{III}/Ga^{III} 12-Metallacrown-4 Complexes Using 1D ^1H NMR and Model Structures

Matteo Melegari, Vittoria Marzaroli, Rosy Polisicchio, Davide Seletti, Luciano Marchiò, Vincent L. Pecoraro,* and Matteo Tegoni*

Cite This: https://doi.org/10.1021/acs.inorgchem.3c00983

Read Online

ACCESS | Metrics & More | Article Recommendations | Supporting Information

ABSTRACT: The solution structure of $Ln^{III}Na^{I}(OBz)_4[12\text{-}MC_{Ga^{III}(N)Shi^{-}}4]$ complexes was studied through paramagnetic ^1H NMR and DFT models. Although isostructural in the solid state, their ^1H NMR spectra in DMSO-d_6 are extremely different from one another due to the magnetic anisotropy of the lanthanide(III) ions. NMR data were analyzed by the "all-lanthanide" method that were compared to X-ray structures and model structures, allowing to establish the extent of the structural changes that occur from the solid state to the solution phase. Major structural changes involve the phenyl groups of the benzoate ions that, quite surprisingly, in solution present preferential orientations lowering the symmetry of the complex contrary to what observed in the solid state. Overall, DFT methods and 1D NMR data allowed us to clarify aspects related to molecular rearrangement processes in solution that could not be predicted by a simple look at the X-ray structures of these complexes.

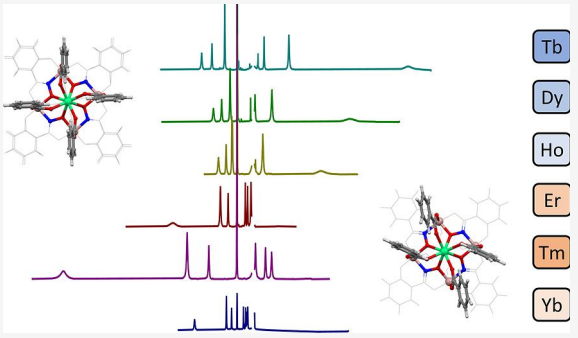

1. INTRODUCTION

Metallacrowns (MCs) are a class of self-assembled complexes that in recent years has gathered attention due to their possible application in the areas of bioimaging, catalysis, single-molecule magnetism, and lanthanide luminescence.[1−14] MCs are the inorganic analogues of crown ethers, in which the $[C-C-O]_n$ repetition unit is replaced by $[M-N-O]_n$. As in their organic counterparts, the oxygen atoms pointing toward the center of the macrocyclic ring are highly preorganized for the complexation of metal cations, from alkali metals to transition ones, to lanthanides and actinides.[15−18]

Lanthanide(III) 12-MC-4 complexes assembled using salicylhydroxamate (Shi^{3-}) and Ga^{III} as the ring metal ($\{Ln^{III}(RO)_4[12\text{-}MC_{Ga^{III}(N)Shi}\text{-}4]\}^{-}$) have very recently received attention for the development of new luminescent molecules.[1,8,19] In these complexes, ancillary carboxylates (RO^{-}) bridge between the core ion and the ring metals, in this way fulfilling the coordination requirements of the lanthanide ions (often found 8-coordinated in these complexes).[8,20,21]

Given their potential especially in biological imaging,[1,8,19] the study of the stability and the structure in solution of these complexes is pivotal. In this context, the presence of a lanthanide ion opens a window on the study of structural investigations in solution of these compounds using ^1H NMR. The analysis of the paramagnetic shift operated by the lanthanide cations, and in particular the pseudocontact (dipolar) contribution, carries truly precious structural information. The presence of a paramagnetic Ln^{III} center produces a shift in the observed resonance frequency of a nucleus in a coordinated ligand (δ_{Ln}^{obs}) that is the sum of a diamagnetic (δ_{Ln}^{dia}) and a paramagnetic contribution (δ_{Ln}^{para}) or lanthanide induced shift. The δ_{Ln}^{para} term is in turn the sum of two contributions: the Fermi-contact contribution, which depends on the electron density of the unpaired electron close to the observed NMR nucleus (δ_{Ln}^{FC}), and the pseudocontact contribution which originates from dipolar interactions between the spin of unpaired electrons and the spin angular momentum of the NMR nucleus (δ_{Ln}^{PC}). Following Bleaney's theory and its approximations, the pseudocontact contribution to the observed chemical is related to the structure of the lanthanide complex through eq 1.[22−26]

$$\delta_{Ln}^{PC}(i) = C_J(Ln)\cdot B_{Ln}\cdot\frac{3\cos^2\theta_i - 1}{r_i^3} \quad (1)$$

where $C_J(Ln)$ is the Bleaney's constant for the examined lanthanide ion and B_{Ln} is the crystal field parameter.[27] The $(3\cos^2\theta_i - 1)/r_i^3$ is often referred to as geometric term or $G(i)$,

Received: March 27, 2023

where i identifies a proton under observation, r_i is the distance between the i proton and the paramagnetic center, and θ_i is the angle between the proton, the paramagnetic center and the principal magnetic axis of the complex (Figure 1). Since Y^{III}-

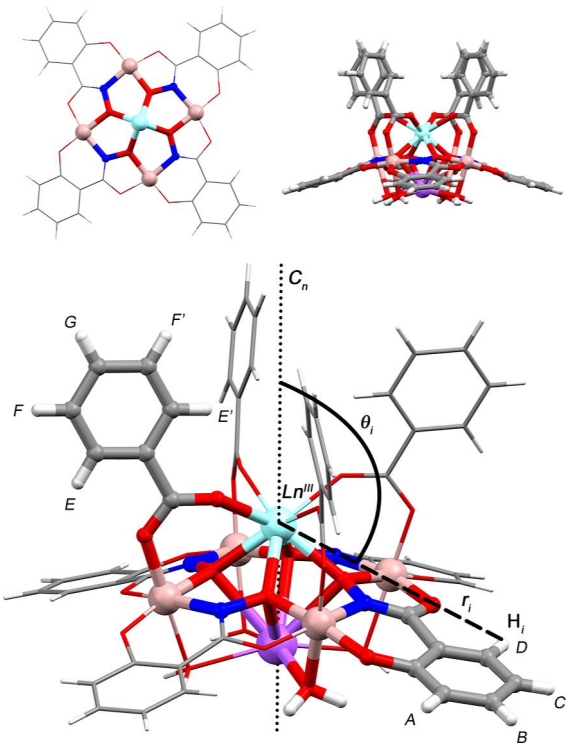

Figure 1. X-ray crystal structure of $Y^{III}Na^{I}(OBz)_4[12\text{-}MC_{GaIII(N)Shi}\text{-}4](H_2O)_4\cdot 6DMF$ complexes (**Y-1**). Top (upper left) and side views (upper right) of the MC scaffold (benzoate residues were excluded in the top view, disordered Shi^{3-} residues and DMF molecules were omitted for clarity). Lower panel: schematic representation of the geometric parameters r_i and θ_i in **Y-1** or **Ln-1** complexes. The principal magnetic axis of the molecule was considered equivalent to the Ln^{III}–Na^{+} direction. Positions labeled with A–G correspond to observable protons in ^{1}H NMR spectra. Cyan: Y^{III}. Brown: Ga^{III}. Purple: Na^{I}.

complexes are usually isostructural with the analogous Ln^{III}-complexes thanks to the similarity in ionic radii, the δ_{Ln}^{para} contribution can be calculated using Y^{III} as the diamagnetic reference ($\delta_{Ln}^{dia} \approx \delta_{Y}^{obs}$)[28,29]

$$\delta_{Ln}^{para}(i) = LIS(i) = \delta_{Ln}^{PC}(i) + \delta_{Ln}^{con}(i) \cong \delta_{Ln}^{obs}(i) - \delta_{Y}^{obs}(i) \quad (2)$$

For an isostructural series of lanthanide complexes such as 12-MC-4, which present a 4-fold axial symmetry, an efficient method of extracting the pseudocontact shift contributions of the Ln^{III} ions from the δ_{Ln}^{para} is the "all lanthanides" method.[30,31] The applicability of this method is general since it does not rely on the Bleaney's constants or their ratio, unlike Reilley's method or most other pseudo-contact/contact shift separation techniques.[32]

As recently reviewed in literature, NMR can be a powerful tool for the evaluation of structural features also for highly paramagnetic MC complexes.[33] Also, we recently and successfully applied the "all lanthanides" method for the analysis of the NMR features of a series of Mn^{III} paramagnetic complexes $Ln^{III}Na^{I}(OAc)_4[12\text{-}MC_{MnIII(N)Shi}\text{-}4](H_2O)_4\cdot 6DMF$ (AcO^{-} = acetate ion), which allowed us to clarify several structural features of the complexes in solution.[31] While this was a significant achievement, the presence of highly paramagnetic Mn^{III} complexes influenced the magnetic properties of the Ln^{III} and therefore a diamagnetic ring metal analogue is necessary to further develop the theory of this system. Furthermore, we have previously observed that the methyl groups in Mn^{III} complexes rotate in solution: since many 12-MC-4 complexes currently under study coordinate aromatic carboxylates, the presence of fluxionality related to these co-ligands deserves to be investigated.

Herein, we report the synthesis and structural characterization, both in solution and in the solid state, of heterotrimetallic $Ln^{III}Na^{I}(OBz)_4[12\text{-}MC_{GaIII(N)Shi}\text{-}4]$ complexes (BzO^{-} = benzoate ion) containing four salicylhydroxamate ligands and four benzoate anions. The lanthanide ions were La^{III}–Lu^{III}, except Ce^{III} and Pm^{III}, and Y^{III}. In particular, we aimed to elucidate the NMR features of these MCs by a deep analysis of their spectra, and to correlate their solid-state structure with structural information obtained through ^{1}H NMR. We also correlated the data obtained from the NMR analysis with the solution structures obtained by computational DFT methods, with the aim of determining the degree of fluxionality and the structural rearrangements occurring in solution. By isolating different lanthanides in the same isostructural host, we were then able to extract parameters that will allow application, in general, of easily accessible 1D ^{1}H NMR data and DFT models, in order to shed light on the structure in solution of lanthanide-containing systems.

2. EXPERIMENTAL SECTION

2.1. Materials and Methods. All reagents and solvents were commercial reagent grade chemicals and used without further purification. Gallium(III) nitrate was considered octa-hydrate ($Ga(NO_3)_3\cdot 8H_2O$), based on studies reported elsewhere.[34] Lanthanide nitrate salts have been used as sources of Ln^{III} ions ($Ln(NO_3)_3\cdot xH_2O$, x = 6 for La^{III}–Gd^{III} and Y^{III}, and x = 5 for Tb^{III}–Lu^{III}). Elemental analysis of the isolated MC batches were performed on Thermofisher Scientific Flash Smart CHNS (sample mass 2–3 mg). Electrospray ionization mass spectra (ESI–MS) of MC complexes (dissolved in methanol) were collected on a Micromass LCT TOF electrospray ionization mass spectrometer, using a capillary voltage of 3500 V and a desolvation temperature of 350 °C. Samples (40 μM) were injected through direct infusion using a syringe pump at 11 μL/min, and the spectra were recorded in full scan analysis mode in the range m/z 100–2000.

2.2. General Preparation of $Ln^{III}Na^{I}(OBz)_4[12\text{-}MC_{Ga^{III}(N)Shi}\text{-}4](H_2O)_y(DMF)_z$ (Ln-1). Salicylhydroxamic acid (30.5 mg, 0.20 mmol) and sodium benzoate (82 mg, 0.57 mmol) were dissolved in 5 mL of a 1:1:0.25 DMF/MeOH/pyridine solution. $Ga(NO_3)_3\cdot 8H_2O$ (80 mg, 0.20 mmol) was dissolved in methanol and added to the solution under stirring. After 5 min, $Ln(NO_3)_3\cdot xH_2O$ (0.05 mmol) was dissolved in 1 mL of methanol, added to the mixture, and stirred for about 5 min. NaCl (50 mg, 0.85 mmol) was dissolved in the minimum quantity of water and 1 mL of methanol and then added to the solution, which was concentrated at RT and left at −4 °C. Slow evaporation of the solvents gave crystals suitable for X-ray diffraction analysis after a couple of days. The complexes were isolated with yields between 10 and 20%. In the complex formula, y (cocrystalized water molecules) resulted 3 for **Dy-1** and 4 for all the other **Ln-1**. The number of cocrystallized DMF molecules (z) was found to be 5 for **Dy-1** and ca. 2 in the bulk (6 in the crystal structures, see below) for all the other **Ln-1** complexes. Results of analyses on **Ln-1** complexes are reported as Supporting Information.

2.3. General Preparation of $Ln^{III}Na^{I}(Op\text{-}Tol)_4[12\text{-}MC_{GaIII(N)Shi}\text{-}4](H_2O)_4(DMF)_5$ (Ln-3). Salicylhydroxamic acid (31 mg, 0.20 mmol) and sodium p-toluenecarboxylate (p-TolONa, 95 mg, 0.57 mmol)

https://doi.org/10.1021/acs.inorgchem.3c00983
Inorg. Chem. XXXX, XXX, XXX–XXX

were dissolved in 5 mL of a 1:1:0.25 DMF/MeOH/pyridine solution. $Ga(NO_3)_3{\cdot}xH_2O$ (80 mg, 0.20 mmol) was dissolved in methanol and added to the solution under stirring. After 5 min, $Ln(NO_3)_3{\cdot}xH_2O$ (0.05 mmol) was dissolved in 1 mL of methanol, added to the mixture, and stirred for about 5 min. NaCl (50 mg, 0.85 mmol) was dissolved in the minimum quantity of water and 1 mL of methanol and then added to the solution, which was concentrated at room temperature and crystalized at −4 °C. Slow evaporation of the solvents gave crystals suitable for X-ray diffraction analysis after a couple of days. The complexes were isolated with yields between 10 and 15%. Results of analyses on **Ln-3** complexes are reported as Supporting Information.

2.4. X-ray Diffractometry. Single crystal X-ray diffraction data of the $Ln^{III}Na^{I}(OBz)_4[12\text{-}MC_{Ga^{III}(N)Shi}\text{-}4](H_2O)_4{\cdot}6DMF$ series (**Ln-1**), where Ln^{III} stands for Ho^{III}, Er^{III}, Lu^{III} and Y^{III}, $Dy^{III}Na^{I}(OBz)_4[12\text{-}MC_{Ga^{III}(N)Shi}\text{-}4](H_2O)_3{\cdot}5DMF{\cdot}3MeOH$ (**Dy-1**), and of $Tb^{III}Na^{I}(Op\text{-}Tol)_4[12\text{-}MC_{Ga^{III}(N)Shi}\text{-}4](H_2O)_4{\cdot}4DMF$ (**Tb-3**), were collected at 150 or 200 K on a Bruker D8 Photon II X-ray diffractometer (Kα(Mo); λ = 0.71073 Å) equipped with a low temperature device. The intensity data were integrated from several series of exposure frames covering the sphere of reciprocal lattice.[35] Absorption correction was applied using the program SADABS.[36] The structures were solved with ShelxT and refined on F^2 with full-matrix least squares (ShelxL), using the Olex2 software package.[37−39] The analysis of the structures (including distances and angles measurements) was carried out using the Mercury 2020.1 software package.[40] In **Y-1**, **Ho-1**, **Er-1**, and **Lu-1**, the salicylhydroximate moiety was found disordered over two positions and refined with site occupancy factors of 0.5 each. Also, in those structures, the presence of cavities was determined, and the solvent was modeled by using the PLATON-SQUEEZE program,[41] which gave voids corresponding approximately to two DMF molecules/cell for each structure. **Y-1**, **Tb-3**, **Ho-1**, and **Lu-1** were refined with suitable twin matrixes. Non-hydrogen atoms were refined with anisotropic thermal parameters. In all complex structures, hydrogen atoms were placed at their calculated positions. A summary of data collection and structure refinement of the complexes presented in this work is reported in Tables S3−S5.

2.5. NMR Spectroscopy. ^{1}H NMR, (1D-, 2D-COSY and PGSE DOSY, Pulsed Gradient Spin Echo), and ^{23}Na NMR spectra were recorded in DMSO-d_6 on a Bruker AVANCE 400 spectrometer, using standard pulse sequences. Diffusion NMR spectra were obtained using a stimulated echo sequence with a bipolar gradient. Chemical shifts (δ, ppm) were referenced to residual DMSO resonances, and the spectral window ranged from −50 to +80 ppm. NMR spectra processing and analysis were performed using the MestreNova 14.1 program.[42] All least-squares regression analyses (calculations through the "all lanthanides" method) were performed using OriginPro 8.[30,43]

2.6. DFT Geometry Optimizations. DFT geometry optimizations were performed using the GAUSSIAN software package.[44] Calculations were performed employing the long range corrected hybrid density functional B3LYP-D3.[45] Solvent effects were included using the SMD model.[46] Geometry optimizations were performed starting from the X-ray experimental geometry of **Y-1** with the exclusion of the Na^+ ion, as it was found to be dissociated from the complex in solution (see below). The crystal structure of **Y-1** exhibited two disordered images, and they were both considered for optimization; however, the model structures converged to the same optimized geometry. One model was optimized changing Y with each lanthanide from La to Lu, except Ce and Pm. MWB46 to MWB60 Large-core Model Core Potentials[47] were used for the lanthanides, MWB28 for Y and Ga, and the systems were treated as pseudo-singlets.[48] The Def2-TZVPP basis set was used for Ga and all the lanthanides, including Y, whereas the 6-31G basis set was used for C, H, N, and O.[49] The model structures of Ln-1 obtained through these calculations are labeled as Ln-DFT.

3. RESULTS AND DISCUSSION

3.1. Molecular Structures. The **Ln-1** complexes of Ho^{III}, Er^{III} and Lu^{III} were analyzed through X-ray diffraction, and the compounds resulted isostructural with **Y-1** in the solid state (Figure 1). The structures are C_4 symmetrical with the Shi^{3-} residues statically disordered over two positions with occupancies 0.5 each. The core Ln^{III} ion is side-on coordinated to the dome shaped MC scaffold at the convex side, with OBz^- ions bridging between the lanthanide and the ring Ga^{III} metal. One Na^+ ion is coordinated on the concave side of the MC. An in-depth description of the structural features of the complexes is reported in the Supporting Information (Figures S1−S14).

In these molecules, we have labeled the hydrogen atoms of the Shi^{3-} ligand with the letters A−D, and the benzoate hydrogen atoms with E−G (Figure 1 and Scheme 1). The Dy^{III} complex, although not isostructural with the other **Ln-1** complexes in the solid state, exhibits only subtle structural differences, i.e., a more flattened MC scaffold and one DMF coordinated to a ring Ga^{III} ion in place of a water molecule.

Scheme 1. Schematic Representation of the Ligands (Left: BzO^-, Right: Shi^{3-}) Used in This Work[a]

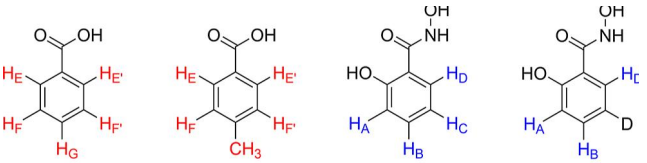

[a]Lettering scheme of protons is reported. The series of complexes for which the ligands are used are reported in italics.

We have also isolated the deuterated analogues of **Ln-1** complexes in which the Shi^{3-} ligand has deuterium in place of ^{1}H in position C (**Ln-2** series), and Ln^{III}[12-MC-4] with *p*-toluate as the bridging carboxylate ligand (**Ln-3** series), for which **Tb-3** presents a solid-state structure analogous to that of the **Ln-1** complexes (the synthesis of **Ln-2** complexes is reported in the Supporting Information).

The structures of the Y^{III}, Dy^{III}, Ho^{III}, Er^{III}, and Lu^{III} complexes were determined by X-ray diffraction. Interestingly, **Lu-1** represents the first lutetium(III) [12-MC_{GaIII}-4] complex to be characterized by X-ray diffraction to date, with the other Lu^{III}-MCs containing Al^{III} (12-MC-4) or Cu^{II} (15-MC-5) as ring metals.[50,51] The complex is isostructural with the other complexes of the **Ln-1** series, as already stated. However, the smaller ionic radius of lutetium(III) makes the $Lu^{III}{-}O_{Bz}$ and $Lu^{III}{-}O_{Shi}$ distances (2.25 and 2.32 Å, respectively) shorter than the same in the other complexes of the series which are in the 2.28−3.31 and 2.34−2.37 Å range, respectively. Also, Lu^{III} is better encapsulated in the cavity compared to the other ions as shown by the smaller displacement from the cavity center. Lu^{III} is in fact 1.45 Å distant from the mean plane of the cavity Shi^{3-} oxygen atoms ($O_{Shi}MP$) compared to 1.46−1.52 Å of the other **Ln-1** structures (Table S2). In-depth structural description of all the complexes is presented in the Supporting Information.

3.2. NMR Characterization. The proton 1D- and 2D-COSY NMR spectra DMSO-d_6 of 13 $Ln^{III}Na^{I}(OBz)_4[12\text{-}MC_{GaIII(N)Shi}\text{-}4](H_2O)_4{\cdot}6DMF$ complexes (**Ln-1**) were examined, where Ln^{III} is $La^{III}{-}Lu^{III}$ (except Ce^{III} and Pm^{III}) and Y^{III}.

https://doi.org/10.1021/acs.inorgchem.3c00983
Inorg. Chem. XXXX, XXX, XXX−XXX

The 1D spectra for **Ln-1** of heavier lanthanides (Ln^{III} = Tb^{III}–Yb^{III}) are reported in Figure 2 along with that of **Y-1**. All

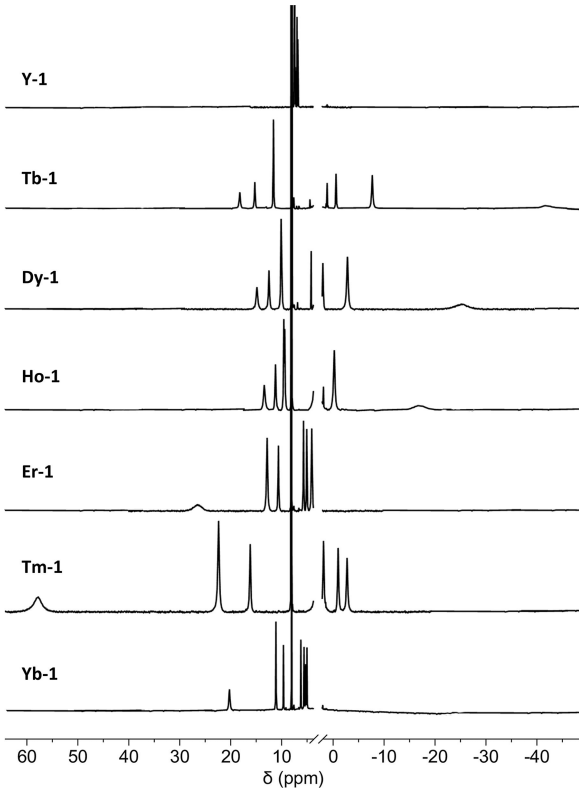

Figure 2. From top to bottom: ^{1}H NMR spectra of **Y-1**, **Tb-1**, **Dy-1**, **Ho-1**, **Er-1**, **Tm-1**, and **Yb-1**. The region 2.00–3.50 ppm is excluded (solvent signals only).

the recorded ^{1}H NMR spectra of the **Ln-1** complexes present a set of seven chemically non-equivalent proton signals as previously observed for the [12-$MC_{MnIII(N)Shi}$-4] analogues, consistent with the presence of an average C_4 symmetry axis in solution. The E/E′ and F/F′ protons (Figure 1) are chemically equivalent, providing information that fast exchange operates for these hydrogen positions. This observation may suggest, at a first glance, that the phenyl rings freely rotate in solution around the C–C bond and that all rotamers around 360° are equally present in solution. However, we will show below that there are orientations of the phenyl rings that are more favored than others, in terms of accessible rotamers, and in fast-exchange regime. This aspect will be discussed in detail in Section 3.5. The ^{1}H NMR spectra of the entire series of **Ln-1** complexes are shown in the Supporting Information (Figures S34–S47).

Due to the paramagnetism of the Ln^{III} ions, the signals spread over a large spectral window that in the case of heavier lanthanides ranges from −40 to +60 ppm. Conversely, the signals of **Y-1**, **La-1**, and **Lu-1** are in the spectral range expected for diamagnetic species and their spectra will be discussed more in detail below (6.50–8.00 ppm, Figure S15). The ^{1}H NMR spectra of **Ln-1** with paramagnetic lanthanides show band widths of ca. 40 Hz (except for **Gd-1**).[a] Therefore, the spectra of these complexes show resolved resonances than those observed previously for the analogues containing Mn^{III}, namely $Ln^{III}Na^I(OAc)_4$[12-$MC_{MnIII(N)Shi}$-4] complexes. Actually, the latter complexes exhibited signals of ca. 500 Hz band width as the result of the relaxation effects operated by the $[Mn^{III}]_4$ system. Also, in the spectra of **Ln-1** with Pr^{III}, Nd^{III}, Sm^{III}, and Eu^{III} the signals are well-resolved, and the H–H coupling constants were observed.[28]

With the purpose of signal assignment (see below) we also registered the spectra of **Ln-2** complexes (Shi^{3-} ligand deuterated in C position), with Ln^{III} being Eu^{III}–Yb^{III} and Y^{III} (Figure 3 for **Y-2**). The ^{1}H NMR spectra of the complexes

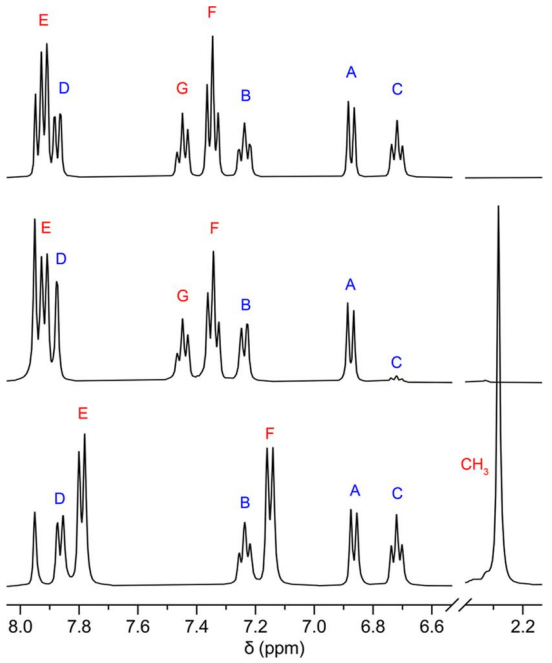

Figure 3. Stacked ^{1}H NMR spectra of **Y-1**, **Y-2**, and **Y-3**. Signals are labeled from A to G and the signals of the Shi^{3-} ligands are highlighted in blue, whereas the signals of the BzO^- or *p*-$TolO^-$ ligands are highlighted in red, see Scheme 1.

are reported as Supporting Information (Figures S48–S55). The ^{1}H NMR spectra are identical to those of **Ln-1** except for the fact that, due to the presence of 85% deuteration on the hydrogen in position C, its resonance has as an integral ca. 15% for **Ln-2** compared to that of **Ln-1** (Figure 3). Finally, we collected the spectra of **Ln-3** complexes, with Ln^{III} being Tb^{III}, Dy^{III}, and Y^{III} (see Supporting Information, Figures S56–S58). The ^{1}H NMR spectra of **Y-3** is also reported in Figure 3: the presence of a signal at 2.28 ppm (CH_3) and the signals pattern provided further information used for signal assignment (see below).

Homonuclear 2D COSY NMR spectra could be examined for **Ln-1**, **Ln-2**, and **Ln-3** complexes with lighter lanthanides only, or Y^{III} (see Supporting Information, Figures S59–S69). We did not observe 2D COSY cross peaks for heavier lanthanides (Tb^{III}–Tm^{III}) as a consequence of the enhanced ^{1}H relaxation conferred by these lanthanide ions.[28] We also acquired PGSE data on **Y-1** which allowed to rule out dissociation phenomena involving BzO^- ions in DMSO (Figure S78). Actually, the normalized intensity of all aromatic signals versus the square of the gradient strength follows the same exponential decay, showing that benzoate and Shi^{3-} ligands are assembled in the same molecular entity in solution, and no appreciable dissociation of benzoate ions is observed (Figure S79).

https://doi.org/10.1021/acs.inorgchem.3c00983
Inorg. Chem. XXXX, XXX, XXX–XXX

Finally, ^{23}Na NMR spectral data were collected for **Ln-1** (Supporting Information, Figures S70−S77). These spectra show that the line widths are in the range from 75 to 90 Hz for **Ln-1**, irrespective of the presence or absence of a paramagnetic lanthanide with similar chemical shift values, which are intermediate between 180 and 500 Hz for the Na^+ adducts with 18-C-6 and 15-C-5 in methanol, and 59 Hz for NaCl in DMSO.[52−55] We, therefore, believe that for our **Ln-1** complexes in DMSO the Na^+ ion is primarily dissociated in solution, as previously observed for $Ln^{III}Na^{I}[12\text{-}MC_{MnIII(N)Shi}\text{-}4](H_2O)_4\cdot 6DMF$ complexes.[31] For these reasons, where referring to compounds **Ln-1** in solution, we will imply sodium dissociation.

3.3. Assignment of Resonances. The first step in the analysis of 1D NMR spectra was to assign all resonances of the diamagnetic complexes to protons A−G (Figure 1). Based on the ^{1}H COSY NMR spectrum of **Y-1** complex, the Shi^{3-} set of signals resulted 6.87, 6.72, 7.24, and 7.87 ppm (Figure 3 and Table S8, Supporting Information), while those of BzO^- resulted 7.34, 7.45, and 7.92 ppm. An unambiguous assignment of the C proton resonance of Shi^{3-} was possible observing the low intensity of the resonance at 6.72 ppm of **Y-2** (85% deuterated, Figure 3). The complete assignment of both Shi^{3-} and benzoate protons was obtained on the basis of signal multiplicity and 2D COSY correlations. An ultimate confirmation of the benzoate protons arose examining the resonances of compound **Y-3** where *p*-$TolO^-$ anions are present in place of BzO^- (i.e., the signal of the G proton at 7.45 ppm is absent in the spectrum of **Y-3** while that of the CH_3 group at 2.28 ppm was observed).

Lu-1 and **Y-1** have almost identical ^{1}H NMR spectra, thus confirming the goodness in the use of the latter as a diamagnetic reference (Table S9 and Figure S15). On the contrary, the ^{1}H NMR spectrum of **La-1** (also diamagnetic) presents significant differences in the position of the signals with respect to that of **Y-1** (Figure S15). Although we may interpret these differences with the tendency of La^{III} to adopt a 9-coordination instead of an 8-coordination, all attempts to crystallize **La-1** were unsuccessful and therefore further discussion is not possible.

The marked differences between the 1D ^{1}H NMR spectra of **Ln-1** of heavier lanthanides (Figure 2) show that the paramagnetic contribution (δ_{Ln}^{para}) is dominant in the observed NMR signals (δ_{Ln}^{obs}) as the result of the large magnetic anisotropy of the core metal. These differences in complexes such as **Tb-1** or **Tm-1** may be up to 50 ppm. This prevented a naked-eye assignment of the resonances for these MCs. Here below we describe the strategy for the assignment of the signals for **Ln-1** of heavier lanthanides, while that for lighter lanthanides is described in the Supporting Information (Pr^{III}−Eu^{III}, Figure S18).

As a first approximation, for each *i* proton in **Ln-1** the $\delta_{Ln}^{para}(i)$ contribution roughly equals $\delta_{Ln}^{PC}(i)$, which considers $\delta_{Ln}^{PC}(i) \gg \delta_{Ln}^{con}(i)$. This, at least for heavier lanthanides, is a sufficiently good approximation given their large Bleaney's constants (eqs 1 and 2). Also, the sign of $\delta_{Ln}^{PC}(i)$ for an *i* proton depends on both the sign of C_J and that of $G(i)$ as shown by eq 1, and therefore the Shi^{3-} and BzO^- signal in each spectrum could be discriminated. Actually, the sign of C_J is known (negative for the oblate Tb^{III}, Dy^{III} and Ho^{III}, positive for the prolate Er^{III}, Tm^{III} and Yb^{III}).[30,56] The evaluation of the crystal structures showed that for the Shi^{3-} protons θ_i are greater than 54.7° and therefore for a prolate ion such as Yb^{III} (i.e., $C_J > 0$) the proton resonances are expected to be upfield shifted with respect to the signals of **Y-1**, which indeed was observed. On the contrary, BzO^- protons θ_i are lower than or close to 54.7° and therefore the three resonances E−G for prolate ions are downfield shifted (both the $G(i)$ term and the Bleaney's constant C_J are positive, Figure S16). The opposite is observed for oblate ions. As a partial result we found that the resonances of the four Shi^{3-} protons are in the spectral windows −3 to +6 ppm for Tb^{III}−Ho^{III} (positive C_J), whereas for Er^{III}−Yb^{III}, which possess a negative C_J, the resonances are observed between +9 and +18 ppm. Conversely, the BzO^- resonances are in the +9 to +57 ppm window for Tb^{III}−Ho^{III}, or in the −42 to +3 ppm window for Er^{III}−Yb^{III} (see Figure S17, Supporting Information).

The final assignment was performed by the evaluation of $\langle G(i)\rangle^b$ values, that are the average value of $G(i)$ over the four corresponding protons in the same *i* position (eight positions for E and F protons) calculated from X-ray crystal data of **Ln-1**

$$\langle G(i)\rangle = \sum (3\cos^2\theta_i - 1)/r_i^3 \quad (3)$$

Since the four Shi^{3-} protons reside at approximately equal θ_i values, it results that the closer a proton is to the lanthanide ion (i.e., the smaller r_i^3) the larger is its associated $\langle G(i)\rangle$ and, therefore, its pseudocontact shift. Based on this information, the largest pseudocontact shift is experienced by the D proton (Table S15), followed by protons A and C. Proton B is the most distant from the Ln^{III} ion, thus experiencing the smallest pseudocontact contribution. These assignments are summarized in Tables S10 and S12 and were confirmed by examination of NMR data of the deuterated **Ln-2** complexes where the signal of C proton is missing. As for the signals of the BzO^- ligands, the peak that experiences the biggest shift (i.e., resonance 1, Figure S16) was assigned to proton E for all compounds, which is the closest to the Ln^{III} ion, thus associated with the largest calculated $\langle G(i)\rangle$ (see Table S10). The resonances of protons F and G were easily assigned by inspection of the peak integrals (two and one protons, respectively).

3.4. Calculation of Pseudocontact Shift. The calculation of the Fermi contact and pseudocontact contributions to the chemical shifts for **Ln-1** complexes was performed using the "all lanthanides" method.[30,31] Data treatment presented here is limited to heavier lanthanides for which the pseudocontact contribution dominates over the Fermi one. However, the treatment for lighter lanthanides is reported in the Supporting Information. Following the "all lanthanides" method, we first plotted the $\delta_{Ln}^{para}(i)$ reported in Table S13 as a function of the reference $\delta_{Yb}^{para}(i)$ (Plot I, Figure 4).[30] Linear regressions forced through the origin were performed on data related to each lanthanide, and the calculated slopes m_{Ln} are reported in Table S14. The physical meaning of m_{Ln} (within the limits of validity of Bleaney's theory) is $m_{Ln} = C_J(Ln)/C_J(Yb)$.[57] However, more realistically, m_{Ln} would reduce to $B_{Ln}C_J(Ln)/B_{Yb}C_J(Yb)$ since B_{Ln} is not expected to be strictly constant throughout the series, as observed for the $Ln^{III}Na^{I}(OAc)_4[12\text{-}MC_{MnIII(N)Shi}\text{-}4](H_2O)_4\cdot 6DMF$ compounds, and C_J values of lanthanides in the complexes may differ from those of the free ions.[31]

Following the "all lanthanides" method, we then plotted the $\delta_{Ln}^{para}(i)/\langle S_z\rangle_{Ln}$ values as a function of $m_{Ln}/\langle S_z\rangle_{Ln}$ (Plot II, Figure 5) in which each line relates to one specific A to G proton. The points were fitted through linear regression

https://doi.org/10.1021/acs.inorgchem.3c00983
Inorg. Chem. XXXX, XXX, XXX−XXX

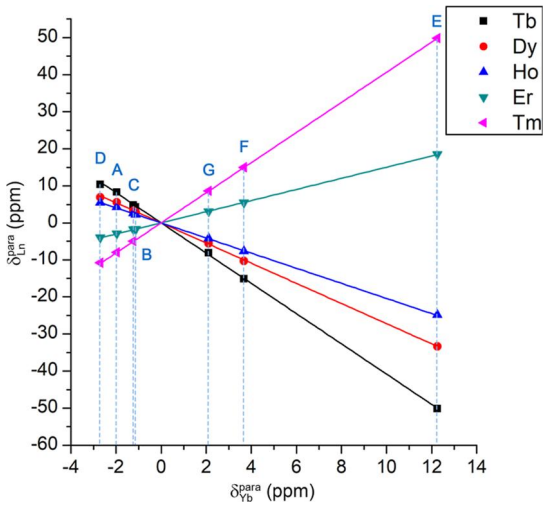

Figure 4. Plot of $\delta_{Ln}{}^{para}(i)$ as a function of $\delta_{Yb}{}^{para}(i)$ ("Plot I") for **Ln-1** (where Ln^{III} = Tb^{III}–Tm^{III}). The A–G labels reported in blue refer to the ligand protons in the corresponding positions.

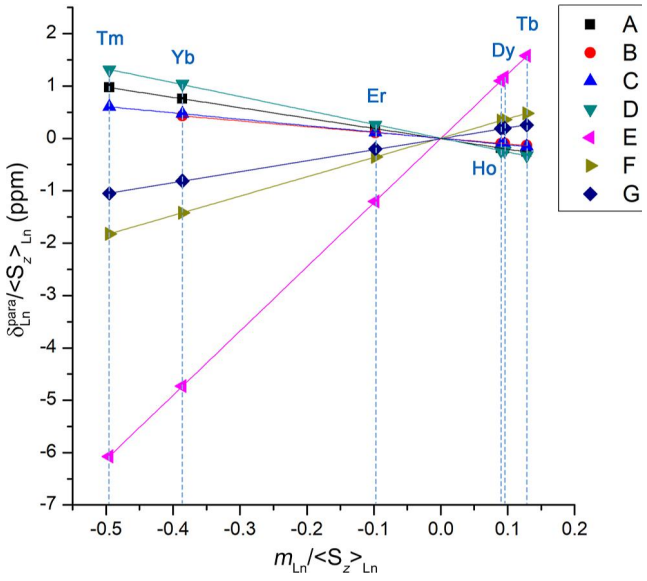

Figure 5. Plot of $m_{Ln}/\langle S_z\rangle_{Ln}$ vs $\delta_{Ln}{}^{para}(i)/\langle S_z\rangle_{Ln}$ ("Plot II") for **Ln-1** (where Ln^{III} = Tb^{III}–Yb^{III}). Letters correspond to proton positions, while $\delta_{Ln}{}^{para}$ values for each lanthanide are on vertical dashed lines.

without constraining the lines passing through the origin. The calculated slope and intercept values, respectively, are labeled M_i and Q_i and are reported in Table S15 and S16.

Pseudocontact and Fermi contact contributions to the chemical shift of the proton signals were then calculated[31]

$$\delta_{Ln}^{PC}(i) = m_{Ln}\cdot M_i \quad (4)$$

$$\delta_{Ln}^{con}(i) = \delta_{Ln}^{obs}(i) - \delta_{Ln}^{PC}(i) \quad (5)$$

The values of $\delta_{Ln}{}^{con}(i)$ and $\delta_{Ln}{}^{PC}(i)$ calculated by means of eqs 4 and 5, respectively are also reported in Tables S15 and S16. Overall, as expected, we found values which confirm that the $\delta_{Ln}{}^{PC}$ contribution dominates over $\delta_{Ln}{}^{con}$. Expectedly, oblate lanthanides (Tb^{III}, Dy^{III}, and Ho^{III}) present $\delta_{Ln}{}^{PC}$ which are opposite in sign than those of prolate ones (Er^{III}, Tm^{III}, and Yb^{III}).

The M_i values determined through the "all lanthanides" method relate with the geometric term $G(i)$ values through the relationship $M_i/M_j = G(i)/G(j)$. Consequently, for each **Ln-1** complex the M_i/M_j ratio obtained by NMR contains the structural information associated to the $G(i)$ parameters. Normalized M_i values (= M_i/M_B, since M_B is the smallest in absolute value) determined by NMR are reported in Table 1 along with the corresponding normalized $G(i)$ values obtained from the crystal structures of **Y-1** and **Er-1** as representative complexes. M_i values should correspond to the $G(i)$ values for a scale factor γ (i.e., $M_i = \gamma\cdot G(i)$) where in theory $\gamma = B_{Ln}\cdot C_J(Yb)$. Here below we will show how we used γ as an empirical least square parameter to compare structural models of the complexes with NMR data. Finally, since the M_i and the $\langle G(i)\rangle$ values have the same sign, the consistency between the NMR observations, the X-ray structural data and the signal assignment are in full agreement.

Noteworthy, the normalized X-ray $\langle G(i)\rangle$ values of Shi^{3-} protons of **Y-1** and **Er-1** (Table 1) are much closer to the corresponding normalized M_i values than those of the benzoate protons (2–23% difference for A–D protons, 24–39% for E–G). Having ruled out the dissociation of benzoates on the basis of PGSE data (Figure S79), we initially made the hypothesis that the larger difference between the M_i and $\langle G(i)\rangle$ values for benzoate protons may arise from the free rotation of the phenyl ring of the BzO^- residues around the C–C axis. A free rotation phenomenon, in fact, is not considered when the X-ray coordinates are used in calculating $\langle G(i)\rangle$. This phenomenon would be indeed similar to that taken into account for the interpretation of NMR data of $Ln^{III}Na^{I}(OAc)_4[12\text{-}MC_{MnIII(N)Shi}\text{-}4](H_2O)_4$ complexes.[31]

We decided therefore to evaluate the presence of free rotation of the phenyl rings to evaluate the NMR data. To this purpose, we generated models based on the X-ray structure of **Y-1** where the phenyl rings are rotated around the C–C axis of 45, 90, and 135° compared to the main benzoate plane (Figure

Table 1. Normalized M_i Values of the Protons Obtained from NMR Data and Normalized Geometric Parameters $\langle G(i)\rangle$ Calculated for the X-ray Structure of Y-1, Ho-1, the Y-rot Model and the Ones of the DFT Models of Y-DFT and Er-DFT[a]

parameter	$i = H_A$	H_B	H_C	H_D	$H_{E/E'}$	$H_{F/F'}$	H_G	σ^b
M_i	1.79	1.00	1.11	2.40	−11.12	−3.35	−1.91	
$\langle G(i)\rangle$								
Y-1	1.56	1.00	1.11	2.05	−7.52	−2.28	−1.21	1.37
Er-1	1.51	1.00	1.14	2.19	−7.67	−2.67	−1.25	1.90
Y-rot	1.56	1.00	1.11	2.05	−2.31	−1.52	−1.21	11.7
Y-DFT	1.62	1.00	1.21	2.62	−9.90	−3.32	−1.91	0.76
Er-DFT	1.62	1.00	1.21	2.63	−10.81	−3.52	−1.99	0.32

[a]The σ values are also reported (see eq 6). [b]See eq 6.

https://doi.org/10.1021/acs.inorgchem.3c00983
Inorg. Chem. XXXX, XXX, XXX–XXX

S20). The corresponding $\langle G(i)\rangle$ parameters were then calculated from eq 3 but as an average of the four models and are reported in Table 1 as **Y-rot**. Surprisingly, for **Y-rot**, the normalized $G(i)$ values for E and F benzoate protons differ by 80 and 55% from the experimental M_i compared to 33 and 32% for the **Y-1** crystal structure, respectively. Strikingly, this result suggests that the free rotation of the phenyl groups is likely not the main cause in the discrepancy between the M_i and $\langle G(i)\rangle$ values for the BzO^- protons. Since the crystal structure of **Y-1** (and of **Er-1**) better explains NMR data compared to the free rotation model, we made the hypothesis that the benzoate aromatic groups instead in a free-rotation situation are rather spatially arranged in preferential positions or conformations, and that these conformations differ from that of the solid state. We therefore decided to investigate the solution structure of those complexes using DFT calculations, in search of other structural models that are consistent with NMR data.

3.5. DFT Model Structures. Starting from the X-ray structure of **Y-1**, models of **Ln-1** complex were generated by replacing Y^{III} with lanthanides (La−Lu, except Pm and Ce). The Na^+ ion was excluded from all models since ^{23}Na NMR data showed that the sodium ion is dissociated in solution. Geometry optimizations were performed on all the models of **Ln-1**, with the output geometries labeled as **Ln-DFT**. The B3LYP-D3 density functional has been used, in order to accurately dispersion effects important in the determination description of non-covalent interactions and isomerization energies. Model **Ln-DFT** structures resulted all very similar, and are reported as Supporting Information. In Figure 6a the representation of the calculated structure for **Er-DFT** is reported, along with the X-ray structure of **Er-DFT**.

Ln-DFT model structures all present a pseudo-C_2 symmetrical conformation. In these structures, two out of the four benzoate ligands are approximately in the same position observed in the X-ray structure, apart from a slight rotation, while the remaining two (in alternate positions) show rotated and tilted phenyl residues which assume a bent conformation with respect to the MC mean plane. These conformational changes of the benzoate ions are accompanied by a slight conformational change of the MC scaffold, in which two alternate Shi^{3-} ligands are more coplanar and the remaining two more bent. Most importantly, CH···π interactions between adjacent BzO^- residues are present in these conformations, in agreement with the hypothesis that the benzoate ligands have preferential rotameric positions in solution.

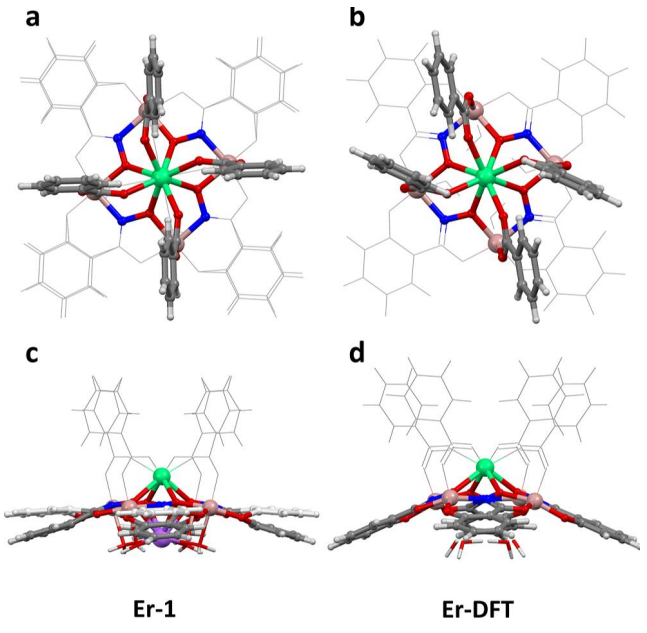

Figure 6. Representation of the conformation of the ligands in the C_4-symmetrical **Er-1** X-ray structure (a,c) and in the pseudo-C_2 **Er-DFT** model (b,d). The pseudo-C_2 symmetry derives from interactions between the benzoate residues and are highlighted in the Supporting Information.

The model structures were evaluated in terms of their consistency with NMR data, along with the C_4 symmetrical crystal structures and the C_4 symmetrical model of **Y-rot** with rotation of the phenyl rings. We calculated the normalized $\langle G(i)\rangle$ (Table 1) and we used the least square function σ (eq 6) for each model structure: the smaller the σ value, the more the structural model is consistent with the NMR data. The scale factor γ in eq 6 was considered a least square parameter.

$$\sigma = \sum_i [M_i - \gamma \cdot \langle G(i)\rangle]^2 \quad (6)$$

The σ parameters are reported in Table 1 along with the normalized M_i and $\langle G(i)\rangle$ of the **Y-1**, **Y-rot**, **Y-DFT**, **Er-1**, and **Er-DFT** models. The $\langle G(i)\rangle$ values for all X-ray structures and DFT models, including calculated γ parameters, are reported in Table S17. Data in Table 1 show that the model structures obtained by DFT are characterized by a better agreement with the NMR data (lower σ values) than both the experimental X-ray structures (**Y-1**, **Er-1**), and the model structure with phenyl rings as free rotamers (**Y-rot**).

As for the conformations adopted by the MC in **Ln-DFT** models, they are characterized by phenyl rings that are interacting with those in adjacent positions, a situation not predictable by inspection of the X-ray structures. Although in these conformations the protons in E/E′ and F/F′ positions are not chemically equivalent, chemical exchange between the two different orientations of the Shi^{3-} e BzO^- in adjacent positions may occur through conformational rearrangement of the MC assembly. Should this rearrangement occur rapidly in solution (i.e., under fast-exchange conditions) together with benzoate rotation around the C−C axis as discussed, then a single value for the chemical shift of each proton is observed in solution, in agreement with the experimental NMR data.

Perhaps not surprisingly, the σ values are lower for the **Ln-DFT** models with heavier lanthanides since the M_i values were obtained through data treatment of the Tb^{III}−Yb^{III} MCs only. The σ values rapidly increase for the **Ln-DFT** models with lighter lanthanides peaking at **La-DFT**, thus supporting our choice to exclude the treatment of lighter lanthanides from the NMR treatment (see Supporting Information).

Further considerations on the nature of these conformers are not possible using the available data. However, it must be highlighted that the presence of multiple stable spatial orientations of the bridging benzoates can be of extreme importance to provide stability to dimeric or trimeric MCs with carboxylate linkers bridging anions.[13,58] Also, the differences in the symmetry of the coordination environment could lead to interesting effects in the luminescent behavior of this class of compounds.[59]

Overall, NMR data analyzed on the basis of crystal and model structures suggest that fluxionality is likely present in these structures. It is worth noting that we cannot exclude that

https://doi.org/10.1021/acs.inorgchem.3c00983
Inorg. Chem. XXXX, XXX, XXX−XXX

a similar fluxionality is present also in the $Ln^{III}Na^{I}(OAc)_4[12\text{-}MC_{MnIII(N)Shi}\text{-}4](H_2O)_4$ complexes we have studied recently. For those complexes, however, the presence of free rotamers related to the acetate CH_3 groups was a model that could explain the NMR data with sufficient precision that no other types of fluxionality or chemical exchange were required to be considered. As for the gallium(III) MCs, our results suggest that the $\{Ln^{III}(OBz)_4[12\text{-}MC_{GaIII(N)Shi}\text{-}4]\}^-$ framework can sustain conformational adaptations that are larger from those predicted by the analysis of the X-ray structures. For these reasons these complexes are expected to be very interesting building blocks for the assembly of complex structures in which the spatial adaptation of the carboxylate ligands is required.

4. CONCLUSIONS

This paper presents an application of both the "all lanthanides" NMR data treatment and DFT calculations to the elucidation of the structural features of a series of self-assembled MCs in solution. The analysis we have performed put together the three groups of information (NMR, DFT, and X-ray structure) to elucidate the nature of structural adaptations that occur in solution. The average four-fold symmetry in solution, consistent with the pattern in the ^1H NMR resonances, is likely not strictly C_4-symmetrical as observed in the solid state. This average four-fold symmetry is rather the result of processes of spatial rearrangement involving both the MC scaffold and the ancillary ligands, presenting two different orientations (also supported by the disorder in the X-ray structures for the salicylhydroximate ligands). The NMR structural information could be rationalized using DFT optimized structures that suggested the presence of intramolecular C−H···π interaction of adjacent benzoate residues leading to C_2-symmetrical MC conformers.

The approach described in this work can be applied in the future to other classes of supramolecules that possess lanthanide ions in their structure. DFT structural models were used to rationalize NMR information that was obtained by a fine treatment of simple 1D data. Also, the "all lanthanides" method allowed for this purpose to process the entire 1D NMR dataset (for heavier lanthanides) as a whole and to extract parameters that are correlated with the structure of lanthanide complexes without incurring in the limitations imposed by other methods of analysis.

■ ASSOCIATED CONTENT

Supporting Information

The Supporting Information is available free of charge at https://pubs.acs.org/doi/10.1021/acs.inorgchem.3c00983.

Experimental procedures for the synthesis of ligands and complexes; experimental details of X-ray structural studies; structural description of the complexes; X-ray crystallographic data; NMR characterization of the complexes (proton 1D and COSY spectra, proton PGSE experiments, ^{23}Na spectra); assignment of the signals for lighter lanthanides; "all lanthanides" method for lighter lanthanides; and results of DFT calculations and representation of the structural models (PDF)

Accession Codes

CCDC 2179628 and 2179795−2179799 contain the supplementary crystallographic data for this paper. These data can be obtained free of charge via www.ccdc.cam.ac.uk/data_request/cif, or by emailing data_request@ccdc.cam.ac.uk, or by contacting The Cambridge Crystallographic Data Centre, 12 Union Road, Cambridge CB2 1EZ, UK; fax: +44 1223 336033.

CCDC 2179628 and 2179795−2179799 contains the supplementary crystallographic data for this paper. These data can be obtained free of charge via www.ccdc.cam.ac.uk/data_request/cif, by emailing data_request@ccdc.cam.ac.uk, or by contacting The Cambridge Crystallographic Data Centre, 12 Union Road, Cambridge CB2 1EZ, UK; fax: +44 1223 336033.

■ AUTHOR INFORMATION

Corresponding Authors

Vincent L. Pecoraro − *Department of Chemistry, Willard H. Dow Laboratories, University of Michigan, Ann Arbor, Michigan 48109, United States;* orcid.org/0000-0002-1540-5735; Email: vlpec@unipr.it

Matteo Tegoni − *Department of Chemistry, Life Sciences and Environmental Sustainability, University of Parma, Parma 43124, Italy;* orcid.org/0000-0002-9621-0410; Email: matteo.tegoni@unipr.it

Authors

Matteo Melegari − *Department of Chemistry, Life Sciences and Environmental Sustainability, University of Parma, Parma 43124, Italy;* orcid.org/0000-0002-7252-7587

Vittoria Marzaroli − *Department of Chemistry, Life Sciences and Environmental Sustainability, University of Parma, Parma 43124, Italy*

Rosy Polisicchio − *Department of Chemistry, Life Sciences and Environmental Sustainability, University of Parma, Parma 43124, Italy*

Davide Seletti − *Department of Chemistry, Life Sciences and Environmental Sustainability, University of Parma, Parma 43124, Italy*

Luciano Marchiò − *Department of Chemistry, Life Sciences and Environmental Sustainability, University of Parma, Parma 43124, Italy;* orcid.org/0000-0002-0025-1104

Complete contact information is available at: https://pubs.acs.org/10.1021/acs.inorgchem.3c00983

Author Contributions

All authors have given approval to the final version of the manuscript. M.T and V.L.P. contributed equally to this work.

Funding

This work was supported by the National Science Foundation under grant CHE-2102046 to V.L.P. The research leading to these results has received funding from the European Community's Seventh Framework Programme (FP7/2013-2017) under grant agreement no. 611488. M.T. and V.L.P. thank the MAECI (Italian Ministry of Foreign Affairs and International Cooperation, Direzione Generale per la Promozione del Sistema Paese) for financial support through the bilateral Italy-USA project "Development of porous magnetic Metallacrowns for sensing applications".

Notes

The authors declare no competing financial interest.

■ ACKNOWLEDGMENTS

This work has benefited from the equipment and framework of the COMP-HUB and COMP-R Initiatives, funded by the "Departments of Excellence" program of the Italian Ministry

for University and Research (MIUR, 2018−2022 and MUR, 2023−2027).

■ ADDITIONAL NOTES

[a]The spectrum of **Gd-1** was recorded but as expected, no peaks of the MC complex were detected due to the extremely short ^{1}H relaxation times induced by the Gd^{III} ion, and only a very broad band was present, approximately from 6 to 9 ppm, apart from those of the solvents. That is again different from what was observed for $Gd^{III}Na^{I}(OAc)_4[12\text{-}MC_{MnIII(N)Shi}\text{-}4]\text{-}(H_2O)_4\cdot 6DMF$ in which the presence of five coupled paramagnetic centers resulted in faster electron relaxation rates for Gd^{III} and, therefore, observable NMR signals.
[b]The ⟨...⟩ brackets mean that the ⟨G(*i*)⟩ parameter was calculated by averaging those of the same *i* positions considering non-symmetry equivalent positions or the presence of disorder and consequent fractional occupancies.

■ REFERENCES

(1) Lutter, J. C.; Eliseeva, S. V.; Kampf, J. W.; Petoud, S.; Pecoraro, V. L. A Unique Ln^{III}{[3.3.1]Ga^{III} Metallacryptate} Series That Possesses Properties of Slow Magnetic Relaxation and Visible/Near-Infrared Luminescence. *Chem.—Eur. J.* **2018**, *24*, 10773−10783.
(2) Lutter, J. C.; Lopez Bermudez, B. A.; Nguyen, T. N.; Kampf, J. W.; Pecoraro, V. L. Functionalization of Luminescent Lanthanide-Gallium Metallacrowns Using Copper-Catalyzed Alkyne-Azide Cycloaddition and Thiol-Maleimide Michael Addition. *J. Inorg. Biochem.* **2019**, *192*, 119−125.
(3) D'Aléo, A.; Pointillart, F.; Ouahab, L.; Andraud, C.; Maury, O. Charge Transfer Excited States Sensitization of Lanthanide Emitting from the Visible to the Near-Infra-Red. *Coord. Chem. Rev.* **2012**, *256*, 1604−1620.
(4) Chow, C. Y.; Eliseeva, S. V.; Trivedi, E. R.; Nguyen, T. N.; Kampf, J. W.; Petoud, S.; Pecoraro, V. L. Ga^{3+}/Ln^{3+} Metallacrowns: A Promising Family of Highly Luminescent Lanthanide Complexes That Covers Visible and Near-Infrared Domains. *J. Am. Chem. Soc.* **2016**, *138*, 5100−5109.
(5) Trivedi, E. R.; Eliseeva, S. V.; Jankolovits, J.; Olmstead, M. M.; Petoud, S.; Pecoraro, V. L. Highly Emitting Near-Infrared Lanthanide "Encapsulated Sandwich" Metallacrown Complexes with Excitation Shifted toward Lower Energy. *J. Am. Chem. Soc.* **2014**, *136*, 1526−1534.
(6) Petoud, S. Novel Antennae for Luminescent Lanthanide Cations Emitting in the Visible and in the Near-Infrared: From Small Molecules to Polymetallic Lanthanide Containing Nanocrystals. *Chimia* **2009**, *63*, 745−752.
(7) Eliseeva, S. V.; Bünzli, J. C. G. Lanthanide Luminescence for Functional Materials and Bio-Sciences. *Chem. Soc. Rev.* **2010**, *39*, 189−227.
(8) Martinić, I.; Eliseeva, S. V.; Nguyen, T. N.; Pecoraro, V. L.; Petoud, S. Near-Infrared Optical Imaging of Necrotic Cells by Photostable Lanthanide-Based Metallacrowns. *J. Am. Chem. Soc.* **2017**, *139*, 8388−8391.
(9) Nguyen, T. N.; Chow, C. Y.; Eliseeva, S. V.; Trivedi, E. R.; Kampf, J. W.; Martinić, I.; Petoud, S.; Pecoraro, V. L. One-Step Assembly of Visible and Near-Infrared Emitting Metallacrown Dimers Using a Bifunctional Linker. *Chem.—Eur. J.* **2018**, *24*, 1031−1035.
(10) Kielar, F.; Law, G. L.; New, E. J.; Parker, D. The Nature of the Sensitiser Substituent Determines Quenching Sensitivity and Protein Affinity and Influences the Design of Emissive Lanthanide Complexes as Optical Probes for Intracellular Use. *Org. Biomol. Chem.* **2008**, *6*, 2256−2258.
(11) Mathieu, E.; Sipos, A.; Demeyere, E.; Phipps, D.; Sakaveli, D.; Borbas, K. E. Lanthanide-Based Tools for the Investigation of Cellular Environments. *Chem. Commun.* **2018**, *54*, 10021−10035.
(12) Lutter, J. C.; Zaleski, C. M.; Pecoraro, V. L. Metallacrowns: Supramolecular Constructs With Potential in Extended Solids, Solution-State Dynamics, Molecular Magnetism, and Imaging. *Adv. Inorg. Chem.* **2018**, *71*, 177−246.
(13) Deb, A.; Boron, T. T.; Itou, M.; Sakurai, Y.; Mallah, T.; Pecoraro, V. L.; Penner-Hahn, J. E. Understanding Spin Structure in Metallacrown Single-Molecule Magnets Using Magnetic Compton Scattering. *J. Am. Chem. Soc.* **2014**, *136*, 4889−4892.
(14) Salerno, E. V.; Kampf, J. W.; Pecoraro, V. L.; Mallah, T. Magnetic Properties of Two $Gd^{III}Fe^{III}_4$ Metallacrowns and Strategies for Optimizing the Magnetocaloric Effect of This Topology. *Inorg. Chem. Front.* **2021**, *8*, 2611−2623.
(15) Pecoraro, V. L.; Stemmler, A. J.; Gibney, B. R.; Bodwin, J. J.; Wang, H.; Kampf, J. W.; Barwinski, A. Metallacrowns: A New Class of Molecular Recognition Agents. *Prog. Inorg. Chem.* **2007**, *45*, 83−177.
(16) Chow, C. Y.; Trivedi, E. R.; Pecoraro, V.; Zaleski, C. M. Heterometallic Mixed 3d-4f Metallacrowns: Structural Versatility, Luminescence, and Molecular Magnetism. *Comments Inorg. Chem.* **2015**, *35*, 214−253.
(17) Ostrowska, M.; Fritsky, I. O.; Gumienna-Kontecka, E.; Pavlishchuk, A. V. Metallacrown-Based Compounds: Applications in Catalysis, Luminescence, Molecular Magnetism, and Adsorption. *Coord. Chem. Rev.* **2016**, *327*−*328*, 304−332.
(18) Lah, M. S.; Pecoraro, V. L. Development of Metallacrown Ethers: A New Class of Metal Clusters. *Comments Inorg. Chem.* **1990**, *11*, 59−84.
(19) Martinić, I.; Eliseeva, S. V.; Nguyen, T. N.; Foucher, F.; Gosset, D.; Westall, F.; Pecoraro, V. L.; Petoud, S. Near-Infrared Luminescent Metallacrowns for Combined: In Vitro Cell Fixation and Counter Staining. *Chem. Sci.* **2017**, *8*, 6042−6050.
(20) Azar, M. R.; Boron, T. T.; Lutter, J. C.; Daly, C. I.; Zegalia, K. A.; Nimthong, R.; Ferrence, G. M.; Zeller, M.; Kampf, J. W.; Pecoraro, V. L.; Zaleski, C. M. Controllable Formation of Heterotrimetallic Coordination Compounds: Systematically Incorporating Lanthanide and Alkali Metal Ions into the Manganese 12-Metallacrown-4 Framework. *Inorg. Chem.* **2014**, *53*, 1729−1742.
(21) Boron, T. T.; Lutter, J. C.; Daly, C. I.; Chow, C. Y.; Davis, A. H.; Nimthong-Roldán, A.; Zeller, M.; Kampf, J. W.; Zaleski, C. M.; Pecoraro, V. L. The Nature of the Bridging Anion Controls the Single-Molecule Magnetic Properties of DyX_4M 12-Metallacrown-4 Complexes. *Inorg. Chem.* **2016**, *55*, 10597−10607.
(22) Bari, L. D.; Pintacuda, G.; Salvadori, P.; Dickins, R. S.; Parker, D. Effect of Axial Ligation on the Magnetic and Electronic Properties of Lanthanide Complexes of Octadentate Ligands. *J. Am. Chem. Soc.* **2000**, *122*, 9257−9264.
(23) del C Fernández-Fernández, M.; Bastida, R.; Macías, A.; Pérez-Lourido, P.; Platas-Iglesias, C.; Valencia, L. Lanthanide(III) Complexes with a Tetrapyridine Pendant-Armed Macrocyclic Ligand: ^{1}H NMR Structural Determination in Solution, X-Ray Diffraction, and Density-Functional Theory Calculations. *Inorg. Chem.* **2006**, *45*, 4484−4496.
(24) Valencia, L.; Martinez, J.; Macías, A.; Bastida, R.; Carvalho, R. A.; Geraldes, C. F. G. C. X-Ray Diffraction and ^{1}H NMR in Solution: Structural Determination of Lanthanide Complexes of a $Py_2N_6Ac_4$ Ligand. *Inorg. Chem.* **2002**, *41*, 5300−5312.
(25) Di Bari, L.; Lelli, M.; Pintacuda, G.; Pescitelli, G.; Marchetti, F.; Salvadori, P. Solution versus Solid-State Structure of Ytterbium Heterobimetallic Catalysts. *J. Am. Chem. Soc.* **2003**, *125*, 5549−5558.
(26) Di Bari, L.; Di Pietro, S.; Pescitelli, G.; Tur, F.; Mansilla, J.; Saá, J. M. $[Ln(binolam)_3]\bullet(OTf)_3$, a New Class of Propeller-Shaped Lanthanide(III) Salt Complexes as Enantioselective Catalysts: Structure, Dynamics and Mechanistic Insight. *Chem.—Eur. J.* **2010**, *16*, 14190−14201.
(27) Bleaney, B. Nuclear Magnetic Resonance Shifts in Solution Due to Lanthanide Ions. *J. Magn. Reson.* **1972**, *8*, 91−100.
(28) Rigault, S.; Piguet, C. Predictions and Assignments of NMR Spectra for Strongly Paramagnetic Supramolecular Lanthanide Complexes: The Effect of the "Gadolinium Break. *J. Am. Chem. Soc.* **2000**, *122*, 9304−9305.
(29) Ouali, N.; Rivera, J.-P.; Morgantini, P.-Y.; Weber, J.; Piguet, C. The Solution Structure of Homotrimetallic Lanthanide Helicates

https://doi.org/10.1021/acs.inorgchem.3c00983
Inorg. Chem. XXXX, XXX, XXX−XXX

Investigated with Novel Model-Free Multi-Centre Paramagnetic NMR methods. *Dalton Trans.* **2003**, *3*, 1251−1263.
(30) Di Pietro, S.; Piano, S. L.; Di Bari, L. Pseudocontact Shifts in Lanthanide Complexes with Variable Crystal Field Parameters. *Coord. Chem. Rev.* **2011**, *255*, 2810−2820.
(31) Atzeri, C.; Marzaroli, V.; Quaretti, M.; Travis, J. R.; Di Bari, L.; Zaleski, C. M.; Tegoni, M. Elucidation of ^{1}H NMR Paramagnetic Features of Heterotrimetallic Lanthanide(III)/Manganese(III) 12-MC-4 Complexes. *Inorg. Chem.* **2017**, *56*, 8257−8269.
(32) Reilley, C. N.; Good, B. W.; Desreux, J. F. Structure-Independent Method for Dissecting Contact and Dipolar NMR Shifts in Lanthanide Complexes and Its Use in Structure Determination. *Anal. Chem.* **1975**, *47*, 2110−2116.
(33) Melegari, M.; Tegoni, M. Aspects of NMR Characterization of Metallacrowns. In *Advances in Metallacrown Chemistry*; Zaleski, C. M., Ed.; Springer International Publishing: Cham, 2022; pp 37−76.
(34) Berbenni, V.; Milanese, C.; Bruni, G.; Marini, A. Thermal Decomposition of Gallium Nitrate Hydrate $Ga(NO_3)_3{\cdot}xH2O$. *J. Therm. Anal. Calorim.* **2005**, *82*, 401−407.
(35) *SMART*; Bruker AXS Inc.: Madison, Wisconsin, 2012.
(36) Krause, L.; Herbst-Irmer, R.; Sheldrick, G. M.; Stalke, D. Comparison of silver and molybdenum microfocus X-ray sources for single-crystal structure determination. *J. Appl. Crystallogr.* **2015**, *48*, 3.
(37) Sheldrick, G. M. SHELXT—Integrated Space-Group and Crystal-Structure Determination. *Acta Crystallogr., Sect. A: Found. Crystallogr.* **2015**, *71*, 3−8.
(38) Sheldrick, G. M. Crystal Structure Refinement with SHELXL. *Acta Crystallogr., Sect. C: Struct. Chem.* **2015**, *71*, 3−8.
(39) Dolomanov, O. V.; Bourhis, L. J.; Gildea, R. J.; Howard, J. A. K.; Puschmann, H. OLEX2: A Complete Structure Solution, Refinement and Analysis Program. *J. Appl. Crystallogr.* **2009**, *42*, 339−341.
(40) Macrae, C. F.; Bruno, I. J.; Chisholm, J. A.; Edgington, P. R.; McCabe, P.; Pidcock, E.; Rodriguez-Monge, L.; Taylor, R.; Van De Streek, J.; Wood, P. A. Mercury CSD 2.0—New Features for the Visualization and Investigation of Crystal Structures. *J. Appl. Crystallogr.* **2008**, *41*, 466−470.
(41) Spek, A. L. PLATON SQUEEZE: A Tool for the Calculation of the Disordered Solvent Contribution to the Calculated Structure Factors. *Acta Crystallogr., Sect. C: Struct. Chem.* **2015**, *71*, 9−18.
(42) Willcott, M. R. MestRe Nova. *J. Am. Chem. Soc.* **2009**, *131*, 13180.
(43) Stevenson, K. J. Review of Originpro 8.5. *J. Am. Chem. Soc.* **2011**, *133*, 5621.
(44) Frisch, M. J.; Trucks, G. W.; Schlegel, H. B.; Scuseria, G. E.; Robb, M. A.; Cheeseman, J. R.; Scalmani, G.; Barone, V.; Petersson, G. A.; Nakatsuji, H.; Li, X.; Caricato, M.; Marenich, A. V.; Bloino, J.; Janesko, B. G.; Gomperts, R.; Mennucci, B.; Hratchian, H. P. *Gaussian 16*, Revision B.01, 2016.
(45) Grimme, S.; Antony, J.; Ehrlich, S.; Krieg, H. A Consistent and Accurate Ab Initio Parametrization of Density Functional Dispersion Correction (DFT-D) for the 94 Elements H-Pu. *J. Chem. Phys.* **2010**, *132*, 154104.
(46) Marenich, A. V.; Cramer, C. J.; Truhlar, D. G. Universal Solvation Model Based on Solute Electron Density and on a Continuum Model of the Solvent Defined by the Bulk Dielectric Constant and Atomic Surface Tensions. *J. Phys. Chem. B* **2009**, *113*, 6378−6396.
(47) Bergner, A.; Dolg, M.; Küchle, W.; Stoll, H.; Preuß, H. Ab Initio Energy-Adjusted Pseudopotentials for Elements of Groups 13−17. *Mol. Phys.* **1993**, *80*, 1431−1441.
(48) Maron, L.; Eisenstein, O. Do f Electrons Play a Role in the Lanthanide-Ligand Bonds? A DFT Study of $Ln(NR_2)_3$; R = H, SiH_3. *J. Phys. Chem. A* **2000**, *104*, 7140−7143.
(49) Hehre, W. J.; Ditchfield, R.; Pople, J. A. Self—Consistent Molecular Orbital Methods. XII. Further Extensions of Gaussian—Type Basis Sets for Use in Molecular Orbital Studies of Organic Molecules. *J. Chem. Phys.* **1972**, *56*, 2257−2261.
(50) Travis, J. R.; Smihosky, A. M.; Kauffman, A. C.; Ramstrom, S. E.; Lewis, A. J.; Nagy, S. G.; Rheam, R. E.; Zeller, M.; Zaleski, C. M. Syntheses and Crystal Structures of Two Classes of Aluminum-Lanthanide-Sodium Heterotrimetallic 12-Metallacrown-4 Compounds: Individual Molecules and Dimers of Metallacrowns. *J. Chem. Crystallogr.* **2021**, *51*, 372−393.
(51) Parac-Vogt, T. N.; Pacco, A.; Nockemann, P.; Yuan, Y. F.; Görller-Walrand, C.; Binnemans, K. Mandelohydroxamic Acid as Ligand for Copper(II) 15-Metallacrown-5 Lanthanide(III) and Copper(II) 15-Metallacrown-5 Uranyl Complexes. *Eur. J. Inorg. Chem.* **2006**, *2006*, 1466−1474.
(52) Delville, A.; Stover, H. D. H.; Detellier, C. Crown Ether-Cation Decomplexation Mechanics. Sodium-23 NMR Studies of the Sodium Cation Complexes with Dibenzo-24-Crown-8 and Dibenzo-18-Crown-6 in Nitromethane and Acetonitrile. *J. Am. Chem. Soc.* **1987**, *109*, 7293−7301.
(53) Lin, J. D.; Popov, A. I. Nuclear Magnetic Resonance Studies of Some Sodium Ion Complexes with Crown Ethers and [2]-Cryptands in Various Solvents. *J. Am. Chem. Soc.* **1981**, *103*, 3773−3777.
(54) Shamsipur, M.; Popov, A. I. Multinuclear NMR Study of Dibenzo-30-Crown-10 Complexes with Sodium, Potassium, and Cesium Ions in Nonaqueous Solvents. *J. Am. Chem. Soc.* **1979**, *101*, 4051−4055.
(55) Colpas, G. J.; Hamstra, B. J.; Kampf, J. W.; Pecoraro, V. L. Preparation of VO^{3+} and VO^{2+} Complexes Using Hydrolytically Stable, Asymmetric Ligands Derived from Schiff Base Precursors. *Inorg. Chem.* **1994**, *33*, 4669−4675.
(56) Rinehart, J. D.; Long, J. R. Exploiting Single-Ion Anisotropy in the Design of f-Element Single-Molecule Magnets. *Chem. Sci.* **2011**, *2*, 2078−2085.
(57) Bleaney, B.; Dobson, C. M.; Levine, B. A.; Martin, R. B.; Williams, R. J. P.; Xavier, A. V. Origin of Lanthanide Nuclear Magnetic Resonance Shifts and Their Uses. *J. Chem. Soc., Chem. Commun.* **1972**, *13*, 791b−793b.
(58) Wang, J.; Lu, G.; Liu, Y.; Wu, S. G.; Huang, G. Z.; Liu, J. L.; Tong, M. L. Building Block and Directional Bonding Approaches for the Synthesis of $\{DyMn_4\}_n$ (n = 2, 3) Metallacrown Assemblies. *Cryst. Growth Des.* **2019**, *19*, 1896−1902.
(59) Eliseeva, S. V.; Salerno, E. V.; Lopez Bermudez, B. A.; Petoud, S.; Pecoraro, V. L. Dy3+ White Light Emission Can Be Finely Controlled by Tuning the First Coordination Sphere of Ga3+/Dy3+ Metallacrown Complexes. *J. Am. Chem. Soc.* **2020**, *142*, 16173−16176.

https://doi.org/10.1021/acs.inorgchem.3c00983
Inorg. Chem. XXXX, XXX, XXX−XXX